THE JOURNAL OF PHYSICAL CHEMISTRY A

Article

pubs.acs.org/JPCA

Conformers, Infrared Spectrum and UV-Induced Photochemistry of Matrix-Isolated Furfuryl Alcohol

C. Araujo-Andrade,*[,†] A. Gómez-Zavaglia,[‡,§] I. D. Reva,[§] and R. Fausto[§,*]

[†]Unidad Académica de Física de la Universidad Autónoma de Zacatecas, Zacatecas, Mexico

[‡]Centro de Investigación y Desarrollo en Criotecnología de Alimentos (Conicet La Plata, UNLP), 1900 La Plata, Argentina

[§]Department of Chemistry, University of Coimbra, 3004-535 Coimbra, Portugal

Supporting Information

ABSTRACT: The infrared spectra of furfuryl alcohol (2-furanmethanol, FFA) were investigated for FFA monomers isolated in low-temperature argon matrices. The structural interpretation of the obtained experimental spectra was assisted by analysis of the molecule's conformational landscape. According to the DFT(B3LYP)/6-311++G(d,p) calculations, five different minimum energy structures were found on the potential energy surface of the molecule. They can be defined by the orientation of the OCCO and CCOH dihedral angles: GG′, GG, TG, TT, GT (G = +gauche, G′ = −gauche, T = trans) and have a symmetry equivalent configuration: GG′ = G′G, GG = G′G′, TG = TG′, GT = G′T. When zero-point energies are taken into account, only three (GG′, GG, and TT) out of the five unique minima correspond to stable structures. The most stable conformer GG′ (OCCO, 72.7°; CCOH, −59.3°), which in gas phase at room temperature accounts for ∼65% of the total population, was the only form isolated in the argon matrices at 14 K. The other two relevant forms convert into conformer GG′ during matrix deposition. The low temperature glassy and crystalline states of FFA were also obtained and their infrared spectra assigned, suggesting the sole existence of the GG′ conformer also in these phases. The photochemical behavior of FFA induced *in situ*, by tunable UV-laser, was also studied. The longest wavelength resulting in photochemical changes in the structure of the irradiated sample was found to be λ = 229 nm. Such UV irradiation of the matrix-isolated FFA led to production of formaldehyde and different isomeric C_4H_4O species. Cycloprop-2-ene-1-carbaldehyde and buta-2,3-dienal (two conformers) are the main initial C_4H_4O photoproducts formed upon short-time excitation at λ = 229 nm. But-3-ynal (two conformers) was the principal photoproduct resulting from prolonged excitation at λ= 229 nm, being consumed upon irradiation at shorter wavelengths (λ < 227.5 nm). Vinyl ketene is produced from FFA in the *trans* conformation and undergoes isomerization to the *cis* form upon irradiation at λ < 227.5 nm. Cyclopropene, propyne, allene, and CO were also identified in the irradiated matrices (in particular at the later stages of irradiation), suggesting that the photoproduced aldehydes partially decarbonylate during the performed photochemical experiments.

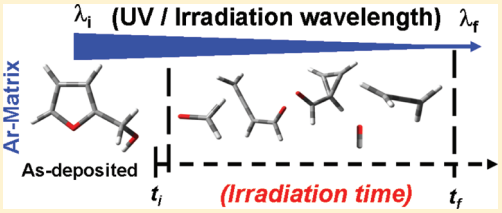

INTRODUCTION

Furfuryl alcohol (FFA; IUPAC name, 2-furanmethanol, also known as furfural alcohol, 2-hydroxymethylfuran, 2-furancarbinol, and α-furylcarbinol) is an organic compound composed by a furan ring substituted with a hydroxymethyl group. It is industrially synthesized from furfural, an industrial chemical derived from a variety of agricultural byproducts, including corncobs, oat and wheat bran, and sawdust. In the presence of an acidic catalyst, FFA undergoes a thermally activated polycondensation process, which leads to linear and branched polymers. Several different mechanisms govern this complex process, which leads to progressive coloration and resinification.[1−5] In addition, FFA is also used as reactive solvent, chemical building block for drug synthesis, and in the manufacture of various chemical products like foundry resins in metal-casting cores and molds, corrosion-resistant materials, polymer concretes, paint strippers and cleaners' formulations, adhesives and wetting agents (surfactants).[6]

John and Radom[7] have carried out *ab initio* studies on FFA with the minimal STO-3G basis set and, based on the rigid rotor approximation, they obtained information about the structures of the predicted conformational isomers of the molecule and their relative stabilities. According to those results, FFA should adopt a nearly perpendicular arrangement of the furan and CH_2OH moieties in preference to coplanar forms.[7] Full relaxed geometry optimizations were later on performed at the same level of theory,[8] and relative energies for five different conformations of FFA were reported. The two lower energy conformations studied were found to have the CCOH fragment in the *trans* (*T*) configuration, the most stable one (in accord with the previous study of John and Radom[7]) possessing perpendicularly oriented furan and CH_2OH moieties.[8] *Gauche* (*G*) forms about the CCOH axis were reported to be at least 4 kJ mol^{-1} higher in energy than the lowest energy structure. Considering the expected possible intramolecular interactions in FFA, which include OH···O and OH···π(C═C) interactions,

Received: December 16, 2011
Revised: February 8, 2012
Published: February 9, 2012

HF/STO-3G calculations are nowadays known not to be accurate enough to properly address the studied system either from the structural or energetic points of views.

Later on, Marstokk and Møllendal[9] carried out an experimental and theoretical study of FFA using microwave spectroscopy at 5 °C and the MP2/6-31G* theoretical approach. The obtained theoretical data led to qualitatively different structural conclusions, when compared with those resulting from the HF/STO-3G calculations.[7,8] In particular, the two lowest energy minima (and not just the lowest energy one as predicted at the HF/STO-3G level) were predicted at the MP2/6-31G* level of theory to have furan and CH_2OH moieties in a *skew* orientation. As in the previous studies,[7,8] the authors concluded on the existence of five different minima, and suggested that the stability of the two lowest energy FFA conformers should be related with the *skew* arrangement of the furan and CH_2OH fragments, which facilitates the establishment of weak OH···O or OH···π(C═C) intramolecular interactions. Experimentally, these two lower energy forms were detected in the microwave spectra of the compound, their measured relative internal energy being 1.5(4) kJ mol^{-1}.[9] No experimental evidence of the presence of further conformers of the molecule was found.

Infrared spectra of FFA in the gaseous and liquid phases and in argon and nitrogen cryomatrices have been reported by Strandman-Long and Murto.[8] The Raman spectrum of the compound in the liquid state has also been investigated[8,10,11] and, in a most recent study, Barsberg and Berg[12] reported a Raman spectroscopic and theoretical study of FFA in weakly interacting environments. The theoretical studies were performed at the DFT/B3LYP level of theory, with different basis sets. In line with previous studies, their main conclusion was that the compound seems to exhibit five conformers. At 298 K, all five forms were predicted to have more than 5% probability, the most abundant forms corresponding to those observed experimentally by Marstokk and Møllendal.[9]

Unfortunately, all previous structural reports on FFA have not investigated the energy barriers for conformational isomerizations, focusing only on the characterization of the minima on the studied potential energy surfaces. Under those circumstances, the stability of the obtained minima could not really be checked. As it will be shown in the present paper, from the five different minimum energy structures of FFA, only three correspond to conformers having practical significance, while the other two correspond to structures that relax barrierlessly to the most stable form, even at 0 K.

All the above-mentioned studies comprise information related with the structural and spectroscopic characteristics of FFA. On the other hand, the information about the photochemistry of the compound is very scarce, and is focused on the role of the compound as singlet oxygen scavenger.[13] The photocatalytic transformation of FFA into 6-hydroxy-(2*H*)-pyran-3-(6*H*)-one in aqueous ZnO suspensions was reported by Richard and Lemaire.[14] In a photolysis-laser-induced fluorescence (LP-LIF) study, gaseous FFA was shown to give rise to $C_4H_3OCH_2$ and OH radicals upon irradiation at 193 nm, with threshold dissociation energy of 357 ± 20 kJ mol^{-1}.[15] To the best of our knowledge, the photochemistry of furfuryl alcohol in rare gas matrices has not been addressed hitherto.

In this work, we present a combined spectroscopic and theoretical study of the structure, vibrational spectra and photochemistry of matrix-isolated furfuryl alcohol, which reveals a new picture regarding the structure and conformational space of the compound. We show that monomeric FFA can adopt only three stable conformations, and not five as believed previously. We also provide insight into the possible unimolecular photoreactions of FFA. Such data is of primary importance for understanding FFA chemical behavior, planning of synthetic routes in which the compound participates, and optimizing its storage and handling procedures. Low temperature infrared spectra of neat FFA in the amorphous and crystalline states were also obtained and interpreted for the first time, indicating the conformational preferences of FFA under these conditions.

■ EXPERIMENTAL AND COMPUTATIONAL METHODS

Infrared Spectroscopy. Furfuryl alcohol ($C_5H_6O_2$) was obtained from Sigma-Aldrich (98% purity). The infrared (IR) spectra were obtained using a Nicolet 6700 Fourier Transform infrared spectrometer equipped with a deuterated triglycine sulfate (DTGS) detector and a Ge/KBr beamsplitter, with 0.5 cm^{-1} spectral resolution. In order to avoid interference from atmospheric H_2O and CO_2, a stream of dry air continuously purged the optical path of the spectrometer. The compound was placed in a specially designed Knudsen cell,[16] whose compartments (sample container and valve nozzle) were kept at room temperature (298 K) during deposition of the matrices. Matrices were prepared by codeposition of furfuryl alcohol vapors coming out of the Knudsen cell together with a large excess of the matrix gas (argon N60, supplied by Air Liquide) onto the CsI substrate of the cryostat cooled to 14 K. The flux of FFA was kept low enough to avoid formation of aggregates (by controlling nozzle valve aperture) and the composition of the sample was monitored, in real time, by periodical recording the IR spectrum of the matrix. The spectra of matrices deposited in such a manner did not evidence the presence of bands due to aggregates. All experiments were performed using an APD Cryogenics closed-cycle helium refrigeration system with a DE-202A expander. After depositing the compound, annealing experiments were performed. The temperature was measured using a Scientific Instruments digital temperature controller with a silicon diode sensor (model 9659) and controlled to within 0.1 K. The temperature variation during the annealing was done in steps of 2 K, up to 32 K, with a duration of 4−5 min per step.

The low temperature solid amorphous layer was prepared in the same way as the matrices, but with the flux of matrix gas cut off. The layer was then allowed to anneal at slowly increasing temperature up to 240 K. IR spectra were collected during this process every 10 to 20 K of temperature change.

Irradiation of the sample was carried out through the outer quartz window of the cryostat, with the frequency-doubled signal beam of the Quanta-Ray MOPO-SL pulsed (10 ns) optical parametric oscillator (fwhm ∼0.2 cm^{-1}, repetition rate 10 Hz, pulse energy ∼4 mJ) pumped with a pulsed Nd:YAG laser. The UV-output of this equipment is tunable down to the limit of 220 nm (the shortest wavelength possible).

Computational Methodology. The quantum chemical calculations were performed with Gaussian 03[17] at the DFT level of theory, using the 6-311++G(d,p) basis set and the three-parameter density functional abbreviated as B3LYP, which includes Becke's gradient exchange correction[18] and the Lee, Yang, and Parr correlation functional.[19]

Structures were optimized using the geometry direct inversion of the iterative subspace (GDIIS) method.[20] In order to assist the analysis of the experimental spectra, vibrational

Table 1. DFT(B3LYP)/6-311++G(d,p) Calculated Electronic Energies (E/E_h), Relative Electronic Energies (ΔE/kJ mol^{-1}), Zero-Point Energies (ZPE/E_h), Relative Zero-Point Corrected Energies (ΔE_{ZPE}/kJ mol^{-1}) and Relative Gibbs Energies at 298 K (ΔG_{298}/ kJ mol^{-1}) for the Different Minima on the FFA Potential Energy Surface and Estimated from Relative Gibbs Energies Gas-Phase Equilibrium Populations of the FFA Conformers (P_{298}, %)[a]

	E	ΔE^b		ZPE	$\Delta E_{ZPE}{}^b$		ΔG_{298}	P_{298}
				Minimum				
GG′ (G′G)	−344.6565160	0.00		0.1002822	0.00		0.00	65.0
GG (G′G′)	−344.6561305	1.01		0.1003433	1.17		1.69	32.8
GT (G′T)	−344.6541134	6.31		0.1000371	5.66		5.57	
TG (TG′)	−344.6549893	4.01		0.1002658	3.96		3.44	
TT (T′T)	−344.6531525	8.83		0.0 998108	7.59		6.61	2.2
				Transition State[c] Around CCOH				
GG′ →GG	−344.6545028	5.29	4.27	0.0996071	3.51	2.34		
GG → GT	−344.6524744	9.60	4.30	0.0996312	7.73	3.24		
GG′ → GT	−344.6538493	7.00	0.69	0.0996983	5.32	−0.21		
TG → TT	−344.6525683	6.36	1.53	0.0995399	4.31	0.79		
				Transition State[c] Around OCCO				
T′T → TT	−344.6531229	0.08	0.08	0.0995193	−0.69	−0.69		
G′G → GG	−344.6513652	13.52	12.51	0.0999780	12.36	11.19		
GT → TT	−344.6525926	3.99	1.47	0.0999786	3.84	1.91		
G′T → GT	−344.6472737	17.96	17.96	0.0993205	16.08	16.08		
G′G → TG	−344.6549296	4.17	0.16	0.1002133	3.98	0.02		
GG → TG	−344.6520650	10.67	7.68	0.0999780	9.71	6.92		

[a]Zero-point energies (ZPE) scaled by 0.978. [b]For transition states, the first column corresponds to energy differences relative to the minimum indicated as reactant, and the second column to that relative to the minimum indicated as product. [c]The reaction coordinate associated with the first four transition states is the internal rotation about the C−O bond; that associated with the last six transition states is the internal rotation around the exocyclic C−C bond.

frequencies were calculated at the same level of theory and the nature of the stationary points on the potential energy surface resulting from optimization was determined by inspection of the corresponding calculated Hessian matrix. The computed harmonic frequencies were scaled by a single factor (0.978) to correct them mainly for the effects of basis set limitations, neglected part of electron correlation and anharmonicity effects. The theoretical normal modes were analyzed by carrying out the potential energy distribution (PED) calculations, performed according to the procedure described in ref 21. Cartesian force constants resulting from the DFT(B3LYP)/6-311++G(d,p) calculations were transformed into the force constants with respect to the molecule fixed internal coordinates. The internal coordinates used in the PED analysis were defined following the recommendations of Pulay et al.[22] Potential energy profiles for internal rotation were calculated performing relaxed scans on the PES along the relevant reaction coordinates, and the transition state structures for conformational interconversion were obtained using the synchronous transit-guided quasi-Newton (STQN) method.[23]

■ RESULTS AND DISCUSSION

FFA Potential Energy Surface Landscape. FFA has two internal rotational axes, $O_5C_1C_9O_{12}$ (OCCO) and $C_1C_9O_{12}H_{13}$ (CCOH), giving rise to different conformers. In agreement with the previous reports,[7−12] after a systematic investigation of the potential energy surface of FFA, five different minimum energy conformations were found (Figure 1), each one having an equivalent-by-symmetry form. Table 1 displays the B3LYP/6-311++G(d,p) calculated relative energies (including zero-point energy corrections) of the different minima found on the molecule's potential energy surface. The optimized geometrical parameters of all the minima are provided as Supporting Information Table S1.

In the present paper, structures are designated by two symbols. The first symbol describes the relative arrangement of the furan and CH_2OH moieties (the OCCO dihedral angle); the second indicates the conformation around the CCOH dihedral angle: G, *gauche* (∼ +60°); G′, *gauche′* (∼ −60°); T, *trans* (∼180°).

The reasons determining the relative stability of the five minimum energy structures of FFA were already addressed before.[9] The lowest energy forms are stabilized by weak OH···O (most stable GG′ form) or OH···π(C═C) interaction (GG and TG forms, which have predicted zero-point corrected relative energies to the most stable form of 1.17 and 3.96 kJ mol^{-1}, respectively) (see Figure 1 and Table 1). According to the relative energies of GG′ and GG forms, the OH···O interaction appears to be energetically slightly more favorable than the OH···π(C═C) one (ca. 1 kJ mol^{-1}; see Table 1). The two higher energy forms (GT and TT) have the OH group pointing away from the ring and do not exhibit any of the stabilizing OH···O or OH···π(C═C) interactions. By comparison of the relative energies within the two pairs of minima (GG, TG) and (GT, TT), which differ essentially in the relative orientation of the furan and CH_2OH fragments, it can be concluded that the *gauche* arrangement of these moieties is energetically favored in relation to the *trans* geometry by ca. 2−3 kJ mol^{-1} (see Table 1).

The most important structural results obtained in the present study came out from the mapping of the potential energy surface of the molecule and the calculation of the transition

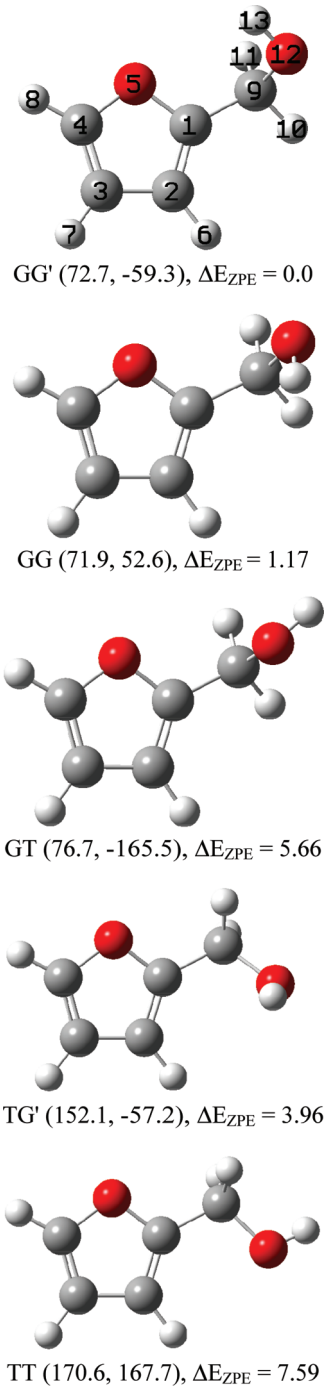

Figure 1. Minimum energy structures on the B3LYP/6-311++G(d,p) potential energy surface of furfuryl alcohol and atom numbering. The calculated equilibrium values for the OCCO and CCOH dihedral angles (degrees) are given in parentheses. The zero-point corrected relative energies (ΔE_{ZPE}/kJ mol^{-1}) are also provided. See also Table 1 for more details. All depicted structures have an equivalent-by-symmetry form. Color codes: red, oxygen; gray, carbon; white, hydrogen.

states for interconversion reactions between the various minima. The calculated potential energy profiles for rotation about the C_9−O_{12} and C_1−C_9 bonds are shown in Figures 2 and 3. In these figures, the zero-point corrected relative energies of the different minima and transition states are also indicated.

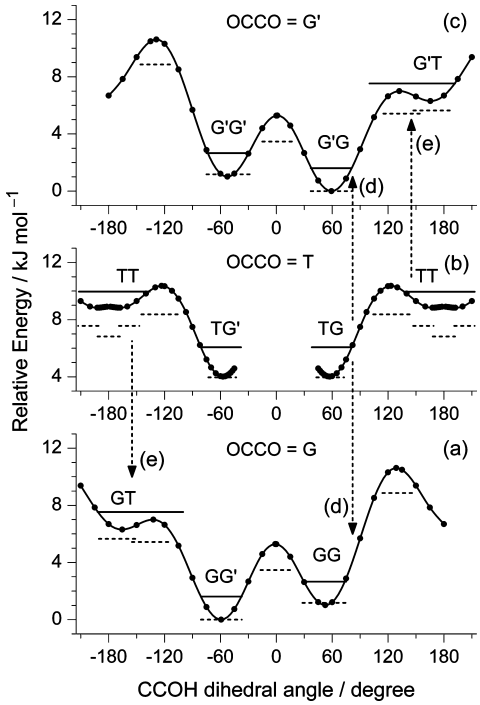

Figure 2. DFT(B3LYP)/6-311++G(d,p) calculated potential energy profiles for the conformational interconversions in FFA resulting from internal rotation about the CCOH dihedral angle. Along the reaction coordinate, the relaxed conformation around the OCCO dihedral angle conserved +Gauche (a), Trans (b) or −Gauche (c) orientation, the CCOH angle was incrementally changed and the remaining coordinates were optimized. The potential energy minima resulting from the internal rotations (a) and (c) are mirror images. Horizontal dashed lines represent the relative energies of the stationary points with the total zero point corrections included (see also Table 1). Horizontal continuous lines represent the energies of the fundamental vibrations along the reaction coordinate (CCOH torsional vibration) for the minima. Vertical dashed arrows across the frames labeled d and e correspond to the potential energy scans along the OCCO dihedral angle that are shown in Figure 3. The discontinuity in frame b between ca. −45° and +45° corresponds to the region of CCOH angles where FFA collapses from T to G (or G′) along the OCCO dihedral angle.

Figure 2 presents the potential energy profiles, corresponding to the internal rotations around the exocyclic C−O bond with the OCCO dihedral angle assuming G′ (Figure 2a), T (Figure 2b) and G′ (Figure 2c) geometries. The most important information taken from this figure is that, when zero-point corrections are taken into account, the energy barriers between TG and GG as well as between G′T and G′G vanish. In practical terms, this means that the TG and G′T minima do not correspond to stable structures. In addition, the zero-point corrected G′G′→G′G barrier is only 2.34 kJ mol^{-1}, which is low enough to be easily overcome during deposition of the low temperature matrices of FFA in the experiments undertaken in this work.[24−26]

The potential energy profiles for internal rotation around the C_1−C_9 bond, when the CCOH geometry is *gauche* and *trans*, are shown in Figure 3. The first profile defines the GG ↔ TG ↔ G′G ↔ GG path (Figure 3d), whereas the second is related with the path for interconversion between the TT and GT forms (Figure 3e). From Figure 3d, it can be concluded that, when zero-point corrections are considered, the TG minimum becomes connected barrierlessly to G′G, i.e., the TG

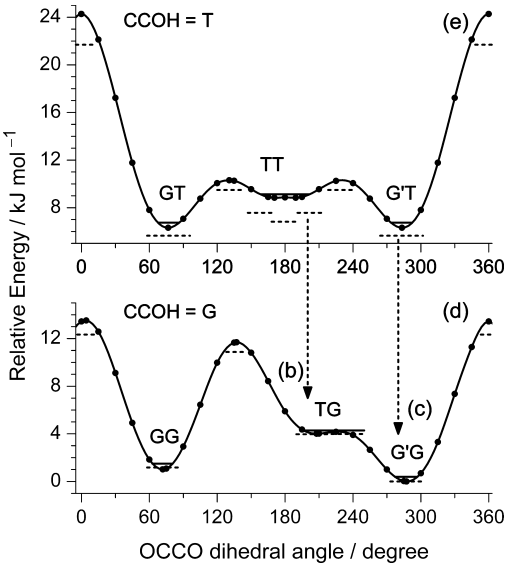

Figure 3. DFT(B3LYP)/6-311++G(d,p) calculated potential energy profiles for the conformational interconversions in FFA resulting from internal rotation about the OCCO dihedral angle. Along the reaction coordinate, the relaxed conformation around the CCOH dihedral angle conserved +Gauche (d) or Trans (e) orientation, the OCCO angle was incrementally changed and the remaining coordinates were optimized. Horizontal dashed lines represent the relative energies of the stationary points with the total zero point corrections included (see also Table 1). Horizontal continuous lines represent the energies of the fundamental vibrations along the reaction coordinate (OCCO torsional vibration) for the minima. Vertical dashed arrows across the frames labeled b and c correspond to the potential energy scans along the CCOH dihedral angle that are shown in Figure 2.

minimum does not correspond to a stable structure in relation to the two internal rotations, around CCOH (Figure 2b) and OCCO (Figure 3d) dihedral angles. Moreover, upon consideration of zero-point corrections, the barrier separating the two equivalent-by-symmetry TT forms also vanishes (see Figure 3e and Figure 2b). In fact, the transition state between the two equivalent TT minima becomes the most probable geometry (having C_s symmetry) in this region of the PES. From Figure 3e it can also be concluded that the TT→GT barrier is low (2.60 kJ mol^{-1}, counted from the C_s symmetry structure; see also Table 1). The additional, alternative relaxation pathway of the TT form may proceed via the initial rotation of the OH group, *i.e.*, *via* the TG form. The related activation barrier is even lower (1.48 kJ mol^{-1}) and, expectably, must be easily accessible during deposition of the matrices in the experiments performed in this study.

In summary, according to the present calculations, only three conformers of FFA shall exist in the gas phase equilibrium: the most stable GG′ conformer and forms GG and TT, the first two forms exhibiting a 2-fold degeneracy and the last one existing as a nondegenerate conformer of C_s symmetry. The expected populations of these conformers at room temperature (~298 K) are then 64.9, 32.8, and 2.2%, respectively (see Table 1). This is in agreement with observation of Marstokk and Møllendal[9] that the GG′ form "makes up most of the gas phase". This, together with the low dipole moment predicted for TT (1.41 D, vs 1.79 and 2.47 D for GG′ and GG, respectively), justifies the observation of only the two most stable FFA conformers in the microwave study.[9] The present investigation of the interconversion pathways between the different FFA minima also demonstrated that the conclusion of Barsberg and Berg[12] that all five different FFA minima should have more than 5% probability in the gas phase equilibrium at room temperature was in fact not correct.

On the other hand, the calculations also allowed us to predict *a priori* that only conformer GG′ should be observable in the low temperature matrices investigated in the present study. In fact, as referred to above, GG can be expected to convert easily during matrix deposition to GG′ (the GG → GG′ barrier is only 2.34 kJ mol^{-1}). On the other hand, TT can easily convert to GT (the TT → GT barrier is 2.60 kJ mol^{-1}) or TG (the TT → TG barrier is 1.48 kJ mol^{-1}), and both GT and TG structures then relaxing barrierlessly to GG′. As shown in the next section, the theoretical prediction of presence of a single conformer of FFA (GG′) in the freshly deposited cryogenic matrices received experimental confirmation.

IR Spectrum of Matrix-Isolated FFA. Figure 4 shows the spectrum of FFA isolated in argon matrix at 14 K. The B3LYP/6-311++G(d,p) calculated spectrum for the three stable FFA conformers are shown for comparison. The complete calculated vibrational data for the relevant conformers of FFA (GG′, GG and TT) are given in Tables S2−S5 (Supporting Information).

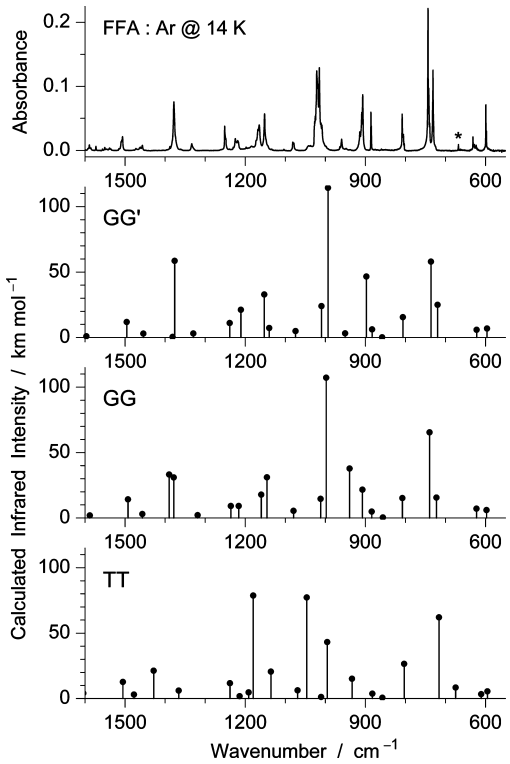

Figure 4. From top to bottom: infrared spectrum of furfuryl alcohol isolated in an argon matrix at 14 K immediately after deposition and B3LYP/6-311++G(d,p) calculated spectra of GG′, GG, and TT conformers. In the calculated spectra, theoretical wavenumbers were scaled by 0.978. In the experimental spectrum, the band marked with asterisk is due to traces of atmospheric CO_2.

As shown in Figure 4, the experimental spectrum fits nicely the calculated spectrum of conformer GG′. The hypothetical presence in the matrix of form TT can be quickly ruled out, since the IR spectrum of this conformer is predicted by the calculations to be considerably different from that of GG′. In particular, the intense TT calculated bands at 1428.5 and

Table 2. Assignment of the IR Spectra of FFA in Argon Matrix, Low Temperature Glassy State, and Crystal[a]

	calculated		experimental			
approx. description	wavenumber	IR intensity	Ar matrix (most stable site)	(less stable sites)	glass (14 K)	crystal (230 K)
νO−H	3744.4	33.8	3641.9	3647.3	3240.7	3219.5
νC_4-H_8	3205.6	0.15	3130.1	n.o.	3148.3	3139.8
νHC_2C_3H s	3180.5	0.16	3126.0	3123.2	3121.7	3118.8
νHC_2C_3H as	3169.7	2.94	3116.9	3115.7	3121.7	3112.2/3092.8
νCH_2 as	3043.2	13.1	2995.3	3006.3/3000.0	2948.3	2973.1
νCH_2 s	2938.9	46.1	2929.5/2878.9	2934.0/2921.6/2888.2/2886.4/2872.4	2927.1/2872.5	2855.9/2829.2/2811.3/2777.0
$\nu C_1{=}C_2$	1596.4	0.91	1600.0	n.o.	1599.0	1598.8
$\nu C_3{=}C_4$	1495.9	11.8	1508.1	1515.3/1509.8/1506.4	1505.2	1503.4
δCH_2	1454.4	2.96	1464.7/1456.9	1472.8/1462.0	1464.5/1446.1/1425.4	1474.0/1448.4/1443.5/1418.7
νC_2-C_3	1381.4	0.44	1387.3	1388.5	1382.7	n.o.
γCH_2	1376.2	58.5	1377.2	1379.0	1361.5	1361.0
$twCH_2$	1329.5	3.04	1332.9	1334.0	1317.7	n.o.
δHC_2C_3H s	1238.5	11.0	1250.0	1251.6/1248.3	1263.9	1264.4/1244.3
νC_1-C_9	1210.6	21.2	1221.6/1216.0	1230.1/1224.8/1218.6	1221.7/1196.2	1226.9/1202.1/1196.3
δCOH	1152.1	32.9	1168.4	1172.6/1170.1/1165.0	1148.5	1153.5/1150.2
δCCH_8	1139.8	7.21	1151.7	1152.5/1147.7	1148.5	1140.3
νC_4-O_5	1074.0	4.90	1078.6	1081.1	1076.9	1078.5
δHC_2C_3H as	1009.1	24.0	1025.1	1027.3/1026.5	1009.4	1026.4/1019.7
νC_9-O_{12}	993.1	114.3	1018.3	1023.1/1021.4/1014.9/1010.7/1008.5	1009.4	997.7/978.6
wCH_2	950.3	3.15	959.3	963.5	956.6	960.0
νO_5-C_1	897.1	46.5	909.0	916.1/913.9/911.0/906.6	914.9	911.0
δ(ring 2)	872.5	6.15	885.2	886.1	884.8	882.1
γHC_2C_3H as	858.0	0.08	859.9	861.3	872.7	872.7
γHC_2C_3H s	806.3	15.4	805.4	808.1/804.8/803.2	820.6	836.2
τ(ring 2)	735.7	57.9	741.5	743.6/739.3	749.8	750.7
γCH_8	719.4	24.9	729.7	732.4/731.5	736.6	738.4/736.0
δ(ring 1)	621.2	5.87	631.3/627.5	632.4/629.0/625.9/621.3	629.7	621.4
τ(ring 1)	596.2	6.85	597.7	599.1	600.1	601.5
δCCO	404.0	14.1	n.i.		420.6	427.0
δOCC	340.2	70.3	n.i.		n.i.	
τC−O	264.1	73.9	n.i.		n.i.	
γC−C	141.8	0.67	n.i.		n.i.	
τC−C	64.3	3.11	n.i.		n.i.	

[a]Wavenumbers in cm^{-1}; IR intensities in km mol^{-1}; ν, bond stretching; δ, bending; tw, twisting; w, wagging; γ, rocking; τ, torsion; s, symmetric; as, asymmetric; n.o., not observed; n.i., not investigated. See Tables S2 and S3 for definition of internal coordinates and full characterization of the normal modes. The B3LYP/6-311++G(d,p) calculated spectrum for conformer GG′ is given for comparison.

1046.3 cm^{-1}, which should be far apart from absorptions of GG′, and can then be considered mark bands of TT, were not observed experimentally. On the other hand, the calculated spectrum of GG does not differ much from that of GG′. Nevertheless, its presence in the matrix can also be ruled out safely: (i) in the 1440−1350 cm^{-1} range, conformer GG is expected to give rise to a doublet of bands (calculated at 1389.7 and 1378.4 cm^{-1}), whereas only a single band is observed experimentally (in agreement with the IR spectrum of GG′); (ii) in the 970−880 cm^{-1} spectral range, both conformers are predicted by calculations to give rise to 3 bands (at 965−940, ∼900 and 885−870 cm^{-1}), but with considerably different intensity patterns, the band intensity ratios being 0.07: 1: 0.13 for GG′ and 1.75: 1: 0.23 for GG. The experimentally observed intensity ratio is 0.12: 1: 0.19, similar to that predicted for GG′ but very different from the one expected for GG; (iii) the two bands at ca. 740 and 730 cm^{-1}, predicted for both conformers, have experimental counterparts which show an intensity ratio of 2.1, in excellent agreement with the intensity ratio calculated for GG′ (2.3; see Table 2) and only about half of that predicted for GG (4.2; see Table S4).

In conclusion, the experimental spectrum of the matrix-isolated FFA confirmed the predictions of the theoretical calculations regarding the trapping of a single conformer of the compound (the most stable GG′ form) in the cryogenic matrix. As expected, both GG and TT conformers, which shall exist in the gas phase prior to deposition, were converted during deposition of the matrix into the most stable GG′ form, to which they are connected by easily accessible energy barriers (*vide supra*).

Most of the bands in the experimental spectrum of matrix isolated FFA exhibit multiplet structures despite the presence of only one conformer in the matrix. This observation indicates that the FFA molecules reside in different local environments (multiple matrix sites) upon isolation in argon. Annealing of the matrix up to 32 K allowed us to convert the less stable sites into a most stable matrix site. These changes were accompanied by the changes in the relative intensities of the individual components of a given band with annealing, being observed throughout the spectrum. Figure 5 shows two representative regions of the difference spectrum obtained by subtracting the IR spectrum of the as-deposited FFA matrix from the spectrum

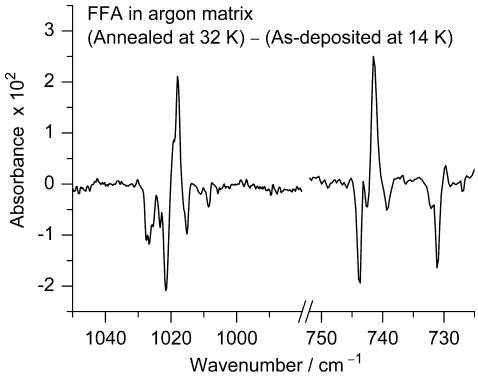

Figure 5. Representative regions of the difference spectrum obtained by subtracting the IR spectrum of freshly deposited sample of FFA in argon (substrate at 14 K) from the spectrum obtained after annealing of the matrix at 32 K.

collected after annealing at 32 K. This figure illustrates the conversion of the less stable matrix sites into the most stable one.

In Table 2, the assignments for the experimental spectrum are presented, including identification of the features ascribable to the most stable and less stable matrix sites.

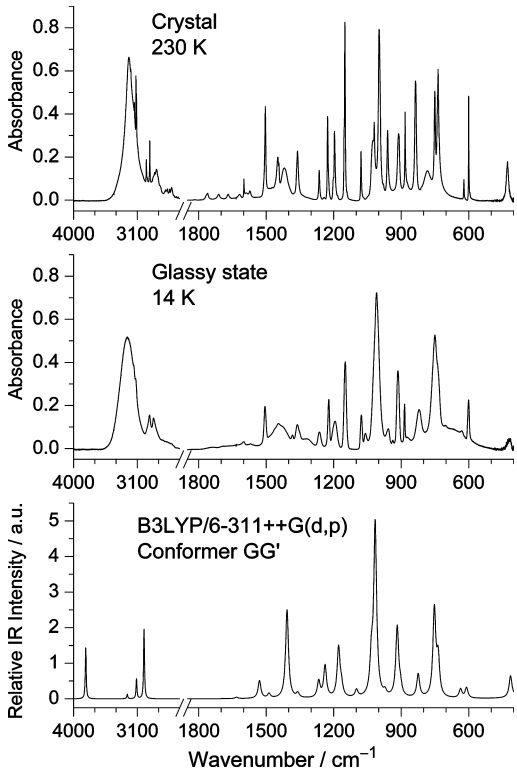

Figure 6. Infrared spectra of FFA in the neat glass and crystalline phases, compared with the simulated spectrum of conformer GG′ (built using Lorentzian functions with a full width at half-maximum of 15 cm^{-1} centered at the scaled calculated B3LYP/6-311++G(d,p) wavenumbers).

Infrared Spectra of FFA in the Low Temperature Neat Crystalline and Glassy States. Figure 6 presents the spectra of FFA in the neat glassy state resulting from deposition of the compound vapor onto the cold substrate (14 K) of the cryostat, and that of the crystalline phase resulting from warming the initially produced glass up to 230 K. Assignments are also presented in Table 2.

As it could be anticipated, the spectrum of the amorphous phase has typically broad bands, due to the significant disorder of this phase. The observed spectrum fits well that simulated using the B3LYP/6-311++G(d,p) calculated data for conformer GG′ (in the simulated spectrum, Lorentzian functions with a full width at half height of 15 cm^{-1} centered at the scaled calculated wavenumbers were used to better mimic the experimental spectrum; the apparent not entirely good agreement observed in a few spectral regions between the experimental and calculated data regarding intensities, results from the different widths of the experimental bands; in the low frequency range, the experimental bands in the 1400 cm^{-1} region, for example, are comparatively broad, so that their relative peak intensity contrasts to that in the simulated spectrum). The good reproduction of the experimental spectrum by the theoretically simulated one, points to the sole presence of conformer GG′ also in the glass prepared as described above, i.e., conformational cooling also occurs during deposition of the neat compound onto the cold substrate of the cryostat.

Upon crystallization of the amorphous phase (at ca. 230 K), the spectrum noticeably changed (see Figure 6). The bands became narrower due to the increase of order, while in some cases they split due to crystal field effects. In spite of its greater complexity, the spectrum of the crystal does not differ considerably from that of the amorphous phase, so that the sole presence of the GG′ form also in the crystalline phase can be postulated. This result must, however, be confirmed, e.g., using the *in situ* cryocrystallization technique together with X-ray crystallography.[27]

Photochemistry of Matrix-Isolated FFA. Matrix-isolated FFA was irradiated with UV light provided by the Nd:YAG/MOPO system, as described in the experimental section. The results are summarized in Figures 7−11. Irradiations with UV

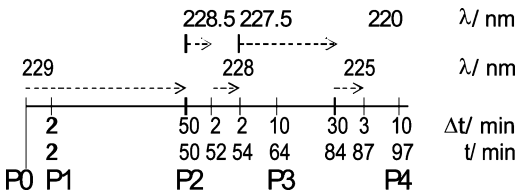

Figure 7. Time line of the irradiation program followed in this study. The spectra collected at stages P0 to P4 were used to build Figures 8−10. P0 designates the reference starting point (as-deposited matrix), i.e., the sample prior to any irradiation. Wavelengths used for irradiation of FFA are shown on top (from 229 to 220 nm). Partial and total irradiation times are pointed out under the time line for each stage of the program.

light λ > 230 nm did not result in any changes of the experimental spectra. When the excitation wavelength was reduced to λ = 229 nm, the bands due to FFA started to decrease. This experimentally found wavelength must correspond to the origin of transition to the first excited singlet state of FFA. This value is in a good agreement with the experimentally observed peak maxima of the UV-spectrum of FFA in the gas phase (E_{max} = 211 nm) and in solution (E_{max} = 218 nm).[28]

From λ = 229 nm, the irradiation wavelength was successively decreased until 220 nm, which is the limit of our laser equipment. The program of the irradiations is shown in Figure 7. In the course of irradiation at λ = 229 nm, consumption

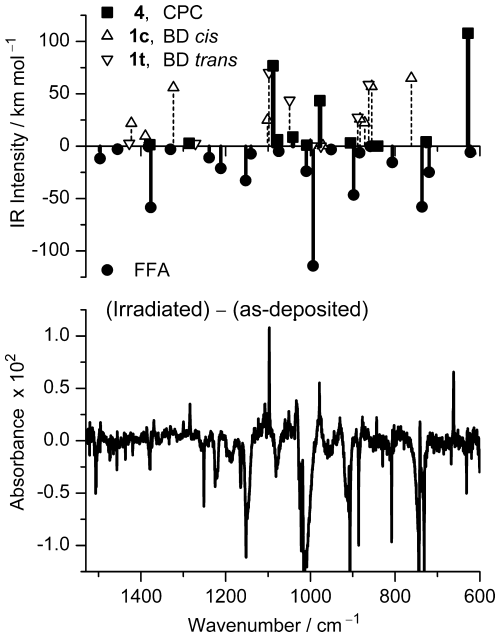

Figure 8. Bottom: difference spectrum obtained as (P1) *minus* (P0). See Figure 7 for positions of P0 and P1 on the timeline of irradiation. Top: B3LYP/6-311++G(d,p) calculated spectra for FFA (GG′ form, negative bands) and selected photoproducts, cycloprop-2-ene-1-carbaldehyde (CPC, **4**) and buta-2,3-dienal (BD; **1c** and **1t**). In the experimental spectrum, the bands observed at 844 and 875 cm^{-1} belong to photoproduced allene. Note that the amount of photoproduced CPC at this stage of irradiation is considerably larger than that of BD, which is stressed by bold drop lines in the calculated spectrum of CPC and thin dashed drop lines for BD.

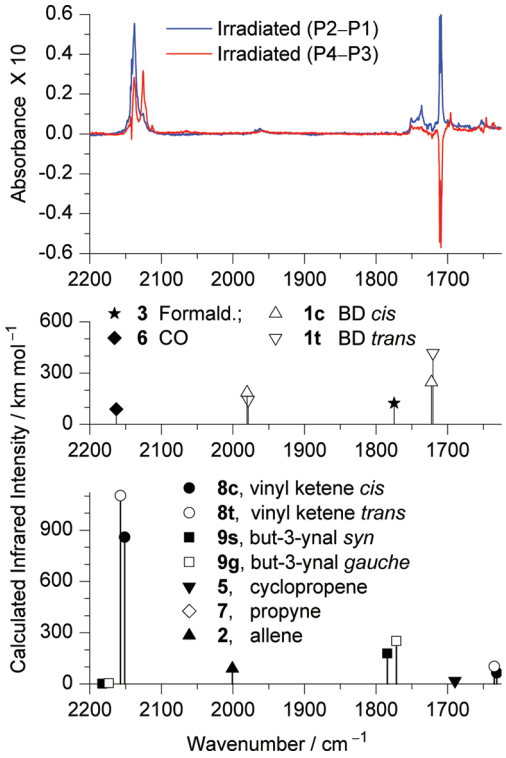

Figure 9. Bottom and Middle: B3LYP/6-311++G(d,p) calculated spectra for main photoproducts observed after irradiation program P2–P4 (see Figure 7). Top: infrared difference spectra (2200–1625 cm^{-1} region). Red: irradiated matrix (P4) *minus* irradiated matrix (P3). Blue: irradiated matrix (P2) *minus* irradiated matrix (P1).

of FFA was accompanied by appearance of new bands. The newly formed bands were found to follow different patterns of variation of intensity along the irradiation, indicating formation of different photoproducts. The spectroscopic data shown in Figures 8–10 allow the identification of the products shown in Figure 11. Assignment of the bands due to the photoproducts is given in Table 3. These assignments take into account: (a) the different patterns of band intensity variations observed along the performed irradiation experiments, (b) the theoretically calculated IR spectra of the possible photoproducts, and also (c) previously reported experimental data on some of these species.

After just 2 min of irradiation at λ = 229 nm, the spectrum of the irradiated sample already showed clearly visible bands due to different photoproducts. The most intense of these bands is a multiplet feature with absolute maximum at 2138 cm^{-1}. The origin of this band will be discussed in detail below. The observed overlapping bands at 1969/1961 and 1956 cm^{-1} appear in the very characteristic wavenumber range of the antisymmetric stretching of the C=C=C moiety.[29] Together with the analysis of the low frequency region of the spectra (see Figure 8), the observation of these bands led to the identification in the irradiated matrix of the two conformers (*cis* and *trans*) of buta-2,3-dienal (**1c, 1t**) and allene (**2**), respectively. The latter gives also rise to the observed bands at 844 and 875 cm^{-1}. In turn, most of the intense bands of buta-2,3-dienal could be identified in the low frequency range spectra, as indicated in Table 3. The presence of formaldehyde (**3**) in the irradiated matrix could also be easily confirmed by observation of the characteristic bands of this compound in

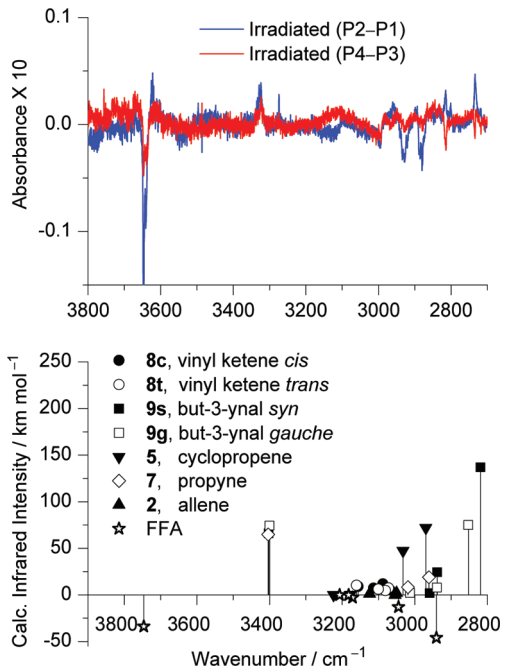

Figure 10. Bottom: B3LYP/6-311++G(d,p) calculated spectra for main photoproducts observed after irradiation programs P2–P4 (see Figure 7). Top: infrared difference spectra (3800–2700 cm^{-1} region). Red: irradiated matrix (P4) *minus* irradiated matrix (P3). Blue: irradiated matrix (P2) *minus* irradiated matrix (P1). Note the shift of the abscissa limits in the experimental vs calculated spectra to improve visual comparison of the two sets of spectra.

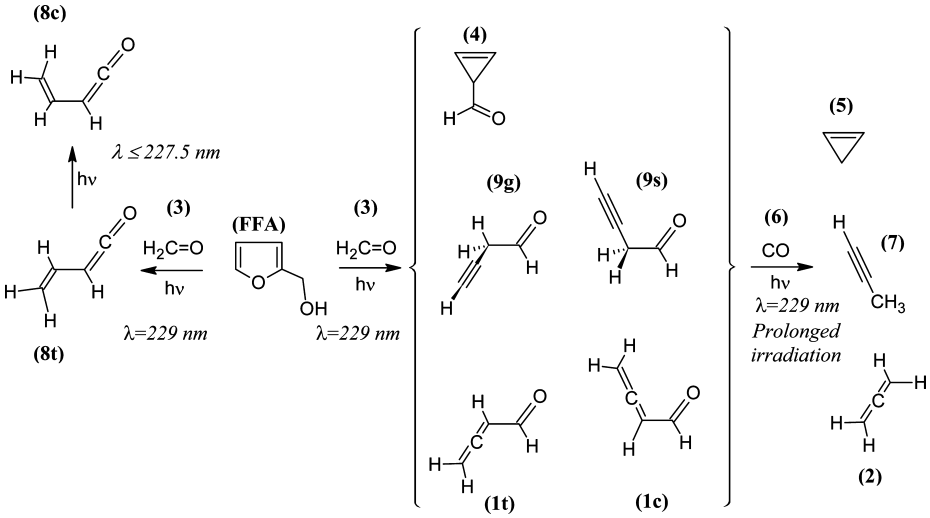

Figure 11. Observed reactions resulting from irradiation of monomeric FFA isolated in an argon matrix. The products are as follows: (*cis/trans*) buta-2,3-dienal (**1c**, **1t**), allene (**2**), formaldehyde (**3**), cycloprop-2-ene-1-carbaldehyde (**4**), cyclopropene (**5**), carbon monoxide (**6**), propyne (**7**), (*trans/cis*) vinyl ketene (**8**), and (*syn/gauche*) but-3-ynal (**9**). The reaction arrows are accompanied by the corresponding wavelengths (λ).

the 1750−1730 cm^{-1} region.[30] Finally, the predicted vibrational signature of *trans* cycloprop-2-ene-1-carbaldehyde (CPC) (**4**) could also be identified in the spectrum upon 2 min of UV (λ= 229 nm) irradiation[31] (see also Table 3).

As it can be observed in Figure 8, according to the relative intensities of the bands due to CPC and to the buta-2,3-dienal forms, at this point of the irradiation program (P1; see Figure 7), the photoproduction of CPC was the dominant reaction (all the most intense observed bands belong to this compound). Most interestingly, the bands due to CPC grew fast and reached nearly their maxima of intensity at this stage of irradiation. Irradiation of the matrix at λ = 229 nm continued for 48 min more, without any significant increase of the intensity of the bands due to CPC, while bands due to the reactant continue to decrease. It can then be concluded that CPC was subsequently transformed in another species. Photodecarbonylation of aldehydes is a well-known process,[32−35] cyclopropene (**5**) being the expected direct product [together with CO (**6**)] of decarbonylation of CPC. Indeed, cyclopropene characteristic bands (e.g., 1658/1656, 1051, 1035/1031, and 921 cm^{-1}) could be observed in the spectra of the irradiated matrix, growing consistently along the λ = 229 nm irradiation. It also appears reasonable to postulate that the observed allene is formed, at least partially, from decarbonylation of buta-2,3-dienal, though phototransformation between cyclopropene and allene (and also propyne (**7**), another C_3H_4 isomer) are well-known processes[30,36] and cannot be discarded to play a role in this case.

In summary, upon irradiation at λ= 229 nm, matrix-isolated FFA undergoes easy fragmentation, with release of formaldehyde and formation of different isomeric C_4H_4O species. CPC and buta-2,3-dienal could be promptly identified by analysis of the low frequency region of the IR spectra of the λ = 229 nm irradiated matrix. Besides, CPC and, with all probability also buta-2,3-dienal, undergo subsequent photodecarbonylation, leading to formation of cyclopropene and allene, whose most characteristic intense bands could also be identified in the IR spectra of the photolyzed matrix.

The origin of the group of overlapping bands with absolute maximum at 2138 cm^{-1} could not be identified just based on the first stages of irradiation. The infrared absorption of CO in argon matrix is known to occur at this wavelength,[35,37] and CO (either isolated or complexed with other products formed simultaneously, e.g., allene or cyclopropene) is certainly one of the contributors to the observed absorptions in this spectral range. However, the data shown in Figure 9 clearly reveal that the main contributor to the absorptions in this range is, with all probability, vinyl ketene (**8c, 8t**). Ketenes give rise to very intense IR bands in this spectral range,[38−42] due to the antisymmetric stretching vibration of the C═C═O group. Vinyl ketene is isomeric with both CPC and buta-2,3-dienal and can then also be formed from FFA, together with formaldehyde. Moreover, it can exist in two stable conformations (*trans* and *cis*, the *trans* form being more stable than the *cis* by 7.4 kJ mol^{-1}, according to the present B3LYP/6-311++G(d,p) calculations). The *trans* form is predicted by the theoretical calculations to possess a ν_{as}C═C═O antisymmetric stretching frequency higher than the *cis* form (2156.2 vs 2150.2 cm^{-1}). Then, the lower frequency bands in this region, emerging at 2125, 2122, and 2113 cm^{-1} upon irradiation of the matrix at the shorter used wavelengths ($\lambda \leq$ 227.5 nm, between points P4 and P3 of the followed irradiation program; see Figure 7) can be ascribed to *cis* vinyl ketene, which was then produced from the most stable *trans* vinyl ketene initially formed upon photolysis of FFA. A few other bands were tentatively assigned to vinyl ketene conformers (see Table 3), though, contrarily to the band due to the ν_{as}C═C═O vibration that is extremely intense in IR (its predicted intensity for *trans* and *cis* vinyl ketene is 1102.4 and 858.9 km mol^{-1}, respectively), the remaining bands of the ketene were predicted to have quite low IR intensities.

Further analysis of Figures 9 and 10 allows one to complete the identification of the products of photolysis of FFA in argon matrix. In the shown spectral regions, the difference spectra represented in the figures (corresponding to differences between the spectra obtained at points P4 and P3 − irradiation at $\lambda \leq$ 227.5 nm—and at points P2 and P1—prolonged irradiation at λ = 229 nm) clearly reveal that the bands observed at 2815, 2734, 2718, 2141, 1711 and 1709/1708 cm^{-1} considerably increase in the P2 − P1 spectrum while they decrease in the P4 − P3 spectrum. This behavior was also observed for other bands in the low frequency spectral range

Table 3. Calculated IR Spectra for the Observed Photoproducts of Matrix-Isolated FFA with Assignments to Experimental Bands[a]

molecule	calculated		experimental	
	wavenumber	IR intensity	this work	literature[b]
CO (**6**)	2163.9	89.2	2138	2138
formaldehyde (**3**)	2876.9	136.0	2873;2865	2873;2863
	2820.2	72.1	2820;2808;2802	2818;2810;2803;2797
	1774.7	123.3	1751;1748;1746;1742; 1740;1738;1736;1732	1752;1742;1740;1738; 1737;1732;1724
	1497.2	9.2	1500;1498;1497	1500;1499;1498
	1232.2	9.3		1248;1245
	1175.9	4.7		1174;1168;1166;1164
(*cis*/*trans*) buta-2,3-dienal (**1**)	3128.0/3127.1	0.3/0.2		
	3071.2/3085.1	4.1/0.0		
	3054.1/3053.1	1.5/0.9		
	2836.7/2850.7	163.7/72.9	2732/2732	
	1980.3/1978.8	186.1/142.9	1969/1961	1965
	1722.4/1720.5	246.6/417.3	1699/1696	1665
	1422.2/1426.9	22.0/2.6	1422/	
	1388.8/1379.2	9.6/0.6		
	1322.6/1270.9	55.9/2.5	1321/1271	
	1100.8/1097.5	25.0/70.1	1112/1107	
	999.8/1048.6	1.1/43.7	/ 1068;1065	
	969.9/995.5	0.5/0.1		
	882.4/974.9	26.1/0.0		
	871.1/887.9	22.3/27.5	877/891	
	854.9/862.1	57.1/58.7	864/870	
	761.4/546.3	65.0/8.1	741/	
	497.2/529.4	2.0/5.2		
	407.3/465.6	4.6/37.3		
	354.4/379.0	5.4/9.9		
	146.2/162.7	10.6/0.8		
	145.2/126.8	5.8/5.4		
cycloprop-2-ene-1-carbaldehyde (**4**)	3237.5	1.9		
	3187.9	5.9		
	3028.8	27.0		
	2790.4	108.0	2722	
	1752.8	170.0	1728;1727;1721;1720	1710
	1697.9	136.1	1670;1668	1696
	1378.1	1.3	1369	
	1285.2	2.7	1284	
	1087.5	76.6	1097	1118
	1076.9	6.1	1091	
	1040.6	8.6	1060	
	1007.7	0.9		
	976.9	43.4	978	978
	904.7	3.0		
	840.5	0.0		
	726.2	4.1		
	627.4	107.9	662	
	507.0	10.3		
	336.5	2.8		
	315.0	4.3		
	130.2	4.5		
(*trans*/*cis*) vinyl ketene (**8**)	3158.9/3154.6	10.3/9.1		3106
	3098.8/3112.2	6.2/7.2		3065
	3079.5/3086.3	4.6/11.8		
	3070.7/3066.6	7.5/5.3		3003

Table 3. continued

molecule	calculated		experimental	
	wavenumber	IR intensity	this work	literature[b]
	2156.2/2150.2	1102.4/858.9	2150;2148;2146;2143; 2138;2133/2125;2122;2113	2137
	1633.9/1630.4	102.5/65.3	1646/1637;1634	1626
	1438.7/1419.6	4.0/13.6	/ 1429	1418
	1329.1/1392.4	0.4/30.8	/ 1398	
	1294.7/1304.7	1.5/0.2		
	1159.4/1120.2	18.9/0.4		1161
	1092.4/1037.0	13.2/8.4	1102/	1102
	986.2/988.3	20.2/15.2		976
	906.7/913.1	2.9/7.6		
	876.5/876.3	59.7/56.6	930/927	875
	695.4/680.6	0.8/9.5		
	623.0/667.1	9.0/0.0		
	550.9/544.8	51.5/57.2	562/560	540
	502.4/498.7	0.4/10.4		
	406.1/424.7	1.8/4.7		
	167.7/141.1	4.0/1.4		
	128.9/80.9	0.1/0.3		
(*syn*/*gauche*) but-3-ynal (**9**)	3400.5/3398.3	66.1/74.2	3328/3328	
	2957.4/3011.5	1.9/1.9		
	2936.6/2937.3	24.3/7.7	2815/2815	
	2817.7/2851.0	136.9/74.9	2718/2734	
	2181.5/2172.4	1.6/4.1	2141/2141	
	1783.4/1770.8	179.0/251.7	1711/1709;1708	
	1405.3/1409.3	17.9/10.1	/ 1436	
	1380.5/1374.9	12.3/6.9		
	1296.0/1265.2	29.3/4.4		
	1208.6/1193.3	0.6/4.8		
	1022.3/1019.5	0.0/0.9		
	995.3/1006.7	10.9/42.8	/ 984;981;976;974;970	
	811.8/954.4	13.4/0.6	792/	
	719.1/714.6	35.1/0.7	711/	
	698.3/683.3	0.6/49.4	/ 663	
	677.5/662.6	48.2/53.3	661/653	
	666.3/494.1	50.0/2.2	657/	
	368.8/456.2	5.1/35.2		
	314.3/322.4	11.7/12.4		
	146.1/174.2	6.0/1.8		
	138.5/60.3	5.1/10.8		
allene (**2**)	3122.8	2.2		
	3052.8	0.0		
	3048.9	2.1		3002
			1997[c]	1999[c]
	2000.0	89.5	1956	1956
	1445.2	0.0		
	1390.7	4.2	1386	1390
	1083.3	0.0		
	994.2	0.4		996
			875[c]	878[c]
	860.7	0.0		
	850.8	129.8	844; 842	844; 839
	364.7	16.4		356; 355
cyclopropene (**5**)	3222.1	0.0		
	3175.9	0.2		
	3030.8	47.3	2980	2980
	2968.0	71.9	2901	2905

Table 3. continued

molecule	calculated		experimental	
	wavenumber	IR intensity	this work	literature[b]
	1688.9	17.5	1658; 1656	1653
	1485.4	1.8		
	1120.8	0.2		
	1082.9	1.4		
	1042.3	25.5	1051	1041
	1004.4	40.4	1035;1031	1012
	989.4	0.0		
	901.9	4.9	921	917
	849.5	0.0		
	764.1	16.7	790	782
	591.5	92.2	599−584	585;580
propyne (7)	3402.3	64.8	3324	3324
	3017.2	16.6	2961	2980
	2959.6	18.9	2949; 2871	2938; 2870
	2173.0	9.6	2141	2138
	1446.2	17.8	1446	1446
	1384.6	0.0		
	1033.0	1.0		
	921.5	0.5		
	655.6	111.8	644;642;640;630;629;625	645;642;630;617
	336.0	21.2		336;335;332

[a]Wavenumbers in cm^{-1}; IR intensities in km mol^{-1}. Calculated wavenumbers were scaled by 0.978. [b]Literature values: CO,[37] formaldehyde,[31] buta-2,3-dienal;[44] CPC,[34] vinyl ketene (gas phase data,[45]), allene,[30] cyclopropene,[34] propyne.[30] [c]Combination band.

(below 1600 cm^{-1}; see Table 3). Altogether, the bands following this pattern of variation with irradiation fit nicely the predicted IR spectra of but-3-ynal (**9**), which is an isomer of CPC, buta-2,3-dienal, and vinyl ketene. But-3-ynal molecule can exist in two conformers, *syn* (**9s**) and *gauche* (**9g**). The *gauche* form is predicted by the B3LYP/6-311++G(d,p) calculations to be more stable than the *syn* form by 4.1 kJ mol^{-1}, and both conformers appear to be present in the photolyzed samples. Consumption of but-3-ynal on the later stages of the irradiation program demonstrates the photolability of this molecule when subjected to irradiation at $\lambda \leq$ 227.5 nm. The expected molecule resulting directly from photolysis of but-3-ynal is propyne (**7**) (together with CO), whose most intense bands could indeed be observed in the photolyzed FFA matrix (see Table 3). As mentioned above, propyne is isomeric of allene and cyclopropene and, once formed, may also photoisomerize to one of these compounds.

In summary, as shown in Figure 11, within the wavelength range used in the present study (229−220 nm), photolysis of matrix isolated FFA initially produces formaldehyde and a series of isomeric molecules of formula C_4H_4O: CPC, buta-2,3-dienal, but-3-ynal, and vinyl ketene. The three photoproduced aldehydes subsequently decarbonylate to the corresponding isomeric C_3H_4 species (cyclopropene, allene, and propyne, respectively), which may also undergo photoinduced interconversions.[30,36] Contrary to the aldehydes, vinyl ketene appears to be photostable once formed. It is initially produced only in the *trans* conformation and is partially converted to the *cis* form upon irradiation at $\lambda \leq$ 227.5 nm.

The UV absorption spectrum of FFA (in a methanol:H_2O_2 20:80 v/v solution) in the 320−200 nm wavelength range was reported by Richard and Lemaire.[14] The absorption maximum occurs at ca. 216 nm, with the longer wavelength band wing extending up to ca. 260 nm. In cyclohexane solution, the band maximum was observed at 218 nm,[28] while in the gas phase spectrum the first absorption band shows its maximum at 211 nm. Hence, all irradiations performed in the present study took place near the first absorption maximum of the compound. According to the literature,[28] this band comprehends the transitions to the two first singlet states, with dominant contribution from the lowest energy transition. Both excited states were proposed to be of π^* character.[28] In agreement with these results, the B3LYP/6-311++G(d,p) calculations yield the HOMO, LUMO and LUMO+1 as being π-type orbitals (Figure S1, Supporting Information) the HOMO−LUMO and HOMO−(LUMO+1) transitions thus being $\pi^* \leftarrow \pi$ transitions. The calculated energies of the LUMO and LUMO+1 orbitals differ only by 0.35 eV (∼34 kJ mol^{-1}), i.e., both orbitals appear to be accessible upon excitation in the wavelength range used in the present study. In addition, the initially formed singlet excited state may undergo intersystem crossing to a triplet state, since two $^3\pi\pi^*$ triplet states were experimentally found to be below the first singlet excited state.[28] Additionally, most of the photoproducts of FFA identified in this study, have their maximum absorption in the 300−170 nm range, corresponding to $\pi-\pi^*$ transitions (see Table S6, Supporting Information).

The excited FFA molecule will then release formaldehyde with simultaneous formation of the C_4H_4O observed isomeric products. Such processes are probably concerted[14] and all of them imply both a hydrogen atom migration from the CH_2OH moiety to the furyl group and the cleavage of the C1−O5 bond. The formation of CPC consists then in a ring contraction similar to that reported previously for furan and both furan-2- and furan-3- carboxaldehydes.[14,33,43,44] As mentioned before, this reaction was found to be the favored one when irradiation of matrix-isolated FFA took place at λ = 229 nm. The formation of all the remaining observed C_4H_4O isomeric forms requires

an additional H atom migration within the C_4H_4O moiety. Finally, it is also interesting to note that the alternative radicalar mechanism involving formation of CH_2OH and furyl radicals seems to be improbable in the light of the present experiments, since its expected main product, furan, could not be observed. Nevertheless, since almost all observed FFA photoproducts have also been reported as products of photodecomposition of furan,[44,46,47] a possible role of this molecule as intermediate in the observed photoprocesses cannot be ruled out and deserves further investigation. A possible alternative explanation for the nonobservation of furan, is that it is produced and quickly consumed under the present irradiation conditions (as suggested previously in the case of the investigation of the photochemistry of matrix isolated 3-furaldehyde[33]). Indeed, furan is known to decarbonylate (with simultaneous production of cyclopropene) already under 253.7 nm UV light excitation in the gas phase.[44,46,47]

CONCLUSION

Matrix isolation IR spectroscopy and DFT(B3LYP)/6-311++G(d,p) calculations allowed a detailed characterization of the structure, conformational landscape, vibrational spectrum, and photochemical behavior of furfuryl alcohol. It was shown that when zero-point energies are taken into account, only three (GG′, GG, TT) out of the five minima on the FFA potential energy surface correspond to stable structures. The most stable conformer GG′ (OCCO, 72.7°; CCOH, −59.3°), was predicted to account for ∼65% of the total population in gas phase at room temperature, while GG and TT should correspond to 32.8 and 2.2%, respectively. At the temperature of the previously reported microwave study of Marstokk and Mollendal[9] (5 °C) the expected relative conformational populations would be 66.2, 31.9, and 1.9%, which, together with the low dipole moment predicted for TT (1.41 D, vs 1.87 and 2.47 D for GG′ and GG, respectively), justifies the observation of only the two most stable FFA conformers in the microwave study. Thus, in the light of the present investigation, the results of the microwave study were finally made compatible with the theoretical predictions (it had been argued that five conformers should contribute to the gas phase equilibrium population with percentages all above 5%[12]).

In agreement with the low calculated energy barriers for conformational interconversion, in the freshly deposited argon matrices only that most stable GG′ conformer could be observed. The other two relevant forms were found to be converted into it during matrix deposition.

The infrared spectra of the low temperature glassy and crystalline states of FFA were also obtained and assigned, suggesting the sole existence of the GG′ conformer also in these phases.

In situ narrow band UV irradiation of the matrix-isolated FFA led to initial formation of formaldehyde and different isomeric C_4H_4O species (cycloprop-2-ene-1-carbaldehyde, but-3-ynal, buta-2,3-dienal and vinyl ketene). Cycloprop-2-ene-1-carbaldehyde and buta-2,3-dienal (2 conformers) are the main initial photoproducts formed upon excitation at the longest wavelength used to irradiate the sample (λ = 229 nm), while but-3-ynal (2 conformers) is the principal photoproduct resulting from prolonged excitation at λ = 229 nm, being consumed upon irradiation at shorter wavelengths ($\lambda \leq 227.5$ nm). Vinyl ketene is produced from FFA in the *trans* conformation and undergoes isomerization to the *cis* form upon irradiation at $\lambda \leq 227.5$ nm. The observed photoprocesses leading to formation of the C_4H_4O isomeric products are probably concerted and all of them imply both a hydrogen atom migration from the CH_2OH moiety to the furyl group and the cleavage of the C1−O5 bond.

Cyclopropene, propyne, allene, and CO were also identified in the irradiated matrices (in particular for the later stages of irradiation), suggesting that the photoproduced aldehydes partially decarbonylate during the performed photochemical experiments.

ASSOCIATED CONTENT

Supporting Information

Figure S1, presenting the highest occupied (HOMO) and the two lowest unoccupied (LUMO; LUMO+1) molecular orbitals for FFA (conformer GG′); Table S1, presenting the B3LYP/6-311++G(d,p) calculated optimized geometries and rotational constants for the five minimum energy structures of FFA; Table S2, presenting the definition of the coordinates used in the normal coordinates analysis of FFA; Tables S3−S5, with the calculated IR spectra and results of the normal coordinates analysis performed for the three conformers of FFA (GG′, GG, and TT); and Table S6, with the UV absorption maxima and type of transitions for the photoproducts of FFA.This material is available free of charge via the Internet at http://pubs.acs.org.

AUTHOR INFORMATION

Corresponding Author

*E-mail: (C.A.-A.) caraujo@fisica.uaz.edu.mx; (R.F.) rfausto@ci.uc.pt.

Notes

The authors declare no competing financial interest.

ACKNOWLEDGMENTS

This work was supported by CYTED (Network 108RT0362), PROMEP (Project UAZ-PTC-092), FCT (Projects PTDC/QUI/71203/2006-FCOMP-01-0124-FEDER-007458 and PTDC/QUI/111879/2009, cofunded by QREN-COMPETE-UE), MinCyT-FCT (Portugal-Argentina bilateral cooperation Grant FCT-MinCyT PO/09/18) and CONACyT (Projects 119491 and 153066). AGZ is member of the Research Career CONICET, Argentina.

REFERENCES

(1) Choura, M.; Belgacem, N. M.; Gandini, A. *Macromolecules* **1996**, *29*, 3839−3850.
(2) Principe, M.; Ortiz, P.; Martinez, R. *Polym. Int.* **1999**, *48*, 637−641.
(3) Chuang, I. S.; Maciel, G. E.; Myers, G. E. *Macromolecules* **1984**, *17*, 1087−1090.
(4) González, R.; Martínez, R.; Ortiz, P. *Makromol. Chem.* **1992**, *193*, 1−9.
(5) González, R.; Figueroa, J. M.; González, H. *Eur. Polym. J.* **2002**, *38*, 287−297.
(6) Gandini, A. In *Encyclopedia of Polymer Science and Engineering*; Mark, H. F., Bikales, N. M., Overberger, C. G., Menges, G., Eds.; Wiley: New York, 1986; Vol. 7, p 454.
(7) John, I. G.; Radom, L. *J. Am. Chem. Soc.* **1978**, *100*, 3981−3991.
(8) Strandman-Long, L.; Murto, J. *Spectrochim. Acta A* **1981**, *37*, 643−653.
(9) Marstokk, K.-M.; Møllendal, H. *Acta Chem. Scand.* **1994**, *48*, 25−31.
(10) Strandman, L. *Acta Chem. Scand. A* **1975**, *29*, 632−636.
(11) Strandman, L. *Acta Chem. Scand. A* **1978**, *32*, 93−93.

(12) Barsberg, S.; Berg, R. W. *J. Phys. Chem. A* **2006**, *110*, 9500−9504.
(13) Haag, W. R.; Hoigné, J.; Gassman, E.; Braun, A. M. *Chemosphere* **1984**, *13*, 631−640.
(14) Richard, C.; Lemaire, J. *J. Photochem. Photobiol. A: Chem.* **1990**, *55*, 127−134.
(15) Chowdhury, P. K.; Upadhyaya, H. P.; Naik, P. D. *Chem. Phys. Lett.* **2001**, *344*, 292−298.
(16) Reva, I. D.; Lopes Jesus, A. J.; Rosado, M. T. S.; Fausto, R.; Eusébio, M. E.; Redinha, J. S. *Phys. Chem. Chem. Phys.* **2006**, *8*, 5339−5349.
(17) Frisch, M. J.; Trucks, G. W.; Schlegel, H. B.; Scuseria, G. E.; Robb, M. A.; Cheeseman, J. R.; Montgomery, J. A., Jr.; Vreven, T.; Kudin, K. N.; Burant, J. C.; et al. Gaussian 03, Revision C.02, Gaussian, Inc.: Wallingford, CT, 2004.
(18) Becke, A. D. *Phys. Rev. A* **1988**, *38*, 3098−3100.
(19) Lee, C. T.; Yang, W. T.; Parr, R. G. *Phys. Rev. B* **1988**, *37*, 785−789.
(20) (a) Csaszar, P.; Pulay, P. *J. Mol. Struct. Theochem* **1984**, *114*, 31−34. (b) Farkas, Ö.; Schlegel, H. B. *Chem. Phys.* **1999**, *111*, 10806−10814.
(21) Rostkowska, H.; Lapinski, L.; Nowak, M. J. *Vib. Spectrosc.* **2009**, *49*, 43−51.
(22) Pulay, P.; Fogarasi, G.; Pang, F.; Boggs, J. E. *J. Am. Chem. Soc.* **1979**, *101*, 2550−2560.
(23) (a) Peng, C.; Schlegel, H. B. *Isr. J. Chem.* **1993**, *33*, 449−454. (b) Peng, C.; Ayala, P. Y.; Schlegel, H. B.; Frisch, M. J. *J. Comput. Chem.* **1996**, *17*, 49−56.
(24) (a) Lopes Jesus, A. J.; Rosado, M. T. S.; Reva, I.; Fausto, R.; Eusébio, M. E.; Redinha, J. S. *J. Phys. Chem. A* **2006**, *110*, 4169−4179. (b) A Lopes Jesus, A. J.; Rosado, M. T. S.; Reva, I.; Fausto, R.; Eusébio, M. E.; Redinha, J. S. *J. Phys. Chem. A* **2008**, *112*, 4669−4678. (c) Rosado, M. T. S.; Lopes Jesus, A. J.; Reva, I. D.; Fausto, R.; Redinha, J. S. *J. Phys. Chem. A* **2009**, *113*, 7499−7507.
(25) Reva, I. D.; Stepanian, S. G.; Adamowicz, L.; Fausto, R. *Chem. Phys. Lett.* **2003**, *374*, 631−638.
(26) (a) Borba, A.; Gómez-Zavaglia, A.; Fausto, R. *J. Mol. Struct.* **2006**, *794*, 196−203. (b) Borba, A.; Gómez-Zavaglia, A.; Simões, P. N. N. L.; Fausto, R. *J. Phys. Chem. A* **2005**, *109*, 3578−3586.
(27) Sharma, A.; Reva, I.; Fausto, R.; Hesse, S.; Xue, Z.; Suhm, M. A.; Nayak, S. K.; Sathishkumar, R.; Pal, R.; Guru Row, T. N. *J. Am. Chem. Soc.* **2011**, *133*, 20194−20207.
(28) Giuliani, A.; Walker, I. C.; Delwiche, J.; Hoffmann, S. V.; Limão-Vieira, P.; Mason, N. J.; Heyne, B.; Hoebeke, M.; Hubin-Franskin, M.-J. *J. Chem. Phys.* **2003**, *119*, 7282−7288.
(29) Jacox, M. E.; Milligan, D. E. *Chem. Phys.* **1974**, *4*, 45−61.
(30) (a) Khoshkhoo, H.; Nixon, E. R. *Spectrochim. Acta* **1973**, *29*, 603−612. (b) Jarmelo, S.; Reva, I. D.; Lapinski, L.; Nowak, M. J.; Fausto, R. *J. Phys. Chem. A* **2008**, *112*, 11178−11189.
(31) CPC may exist in two conformations (*cis* and *trans*, according to the orientation of the cyclopropene ring relatively to the C═O bond), the *trans* conformer being 5.6 kJ mol^{-1} more stable than the *cis* form and the sole form identified in the irradiated matrix of FFA.
(32) Giuliano, B. M.; Reva, I.; Fausto, R. *J. Phys. Chem. A* **2010**, *114*, 2506−2517.
(33) Kuş, N.; Sharma, A.; Reva, I.; Lapinski, L.; Fausto, R. *J. Phys. Chem. A* **2010**, *114*, 7716−7724.
(34) Kuş, N.; Reva, I.; Fausto, R. *J. Phys. Chem. A* **2010**, *114*, 12427−12436.
(35) Lopes, S.; Gómez-Zavaglia, A.; Lapinski, L.; Fausto, R. *J. Phys. Chem. A* **2005**, *109*, 5560−5570.
(36) Hiraoka, H.; Srinivasan, R. *J. Chem. Phys.* **1968**, *48*, 2185−2189.
(37) Dubost, H.; Marguin, L. A. *Chem. Phys. Lett.* **1972**, *17*, 269−273.
(38) Breda, S.; Reva, I.; Lapinski, L.; Fausto, R. *Phys. Chem. Chem. Phys.* **2004**, *6*, 929−937.
(39) S. Breda, S.; Reva, I.; Fausto, R. *Vibrat. Spectrosc.* **2009**, *50*, 57−67.
(40) Kuş, N.; Breda, S.; Fausto, R. *J. Mol. Struct.* **2009**, *924−926*, 81−88.
(41) Reva, I.; Nowak, M. J.; Lapinski, L.; Fausto, R. *Chem. Phys. Lett.* **2008**, *452*, 20−28.
(42) Kuş, N.; Breda, S.; Reva, I.; Tasal, E.; Ogretir, C.; Fausto, R. *Photochem. Photobiol.* **2007**, *83*, 1237−1253; Erratum. *Photochem. Photobiol.* **2007**, *83*, 1541−1542.
(43) Rendall, W. A.; Torres, M.; Strausz, O. P. *J. Org. Chem.* **1985**, *50*, 3034−3038.
(44) Rendall, W. A.; Clement, A.; Torres, M.; Strausz, O. P. *J. Am. Chem. Soc.* **1986**, *108*, 1691−1692.
(45) Bjarnov, E. *Z. Naturforsch.* **1979**, *34A*, 1269−1274.
(46) Srinivasan, R. *J. Am. Chem. Soc.* **1967**, *89*, 1758−1758.
(47) Rendall, W. A.; Torres, M.; Lown, E. M.; Strausz, O. P. *Rev. Chem. Intermed.* **1986**, *6*, 335−364.